

## RESEARCH ARTICLE

# LIM protein Ajuba promotes liver cell proliferation through its involvement in DNA replication and DNA damage control

Noëlle Dommann , Jacopo Gavini, Daniel Sánchez-Taltavull, Felix Alexander Baier, Fabienne Birrer, Giulio Loforese, Daniel Candinias and Deborah Stroka 

Department of Visceral Surgery and Medicine, Inselspital, Bern University Hospital, University of Bern, Bern, Switzerland

## Correspondence

D. Stroka, Department of Visceral Surgery and Medicine, Department of Clinical Research, University of Bern, Murtenstrasse 35, 3008 Bern, Switzerland  
 Tel: +41 31 632 27 48  
 E-mail: [deborah.stroka@dbmr.unibe.ch](mailto:deborah.stroka@dbmr.unibe.ch)

(Received 7 December 2021, revised 31 March 2022, accepted 11 April 2022, available online 15 June 2022)

doi:10.1002/1873-3468.14371

Edited by Ivan Sadowski

**The LIM-domain protein Ajuba is associated with cell proliferation, a fundamental process of tissue regeneration and cancer. We report that in the liver, Ajuba expression is increased during regeneration and in tumour cells and tissues. Knockout of Ajuba using CRISPR/Cas9 is embryonic lethal in mice. shRNA targeting of Ajuba reduces cell proliferation, delays cell entry into S-phase, reduces cell survival and tumour growth *in vivo* and increases expression of the DNA damage marker  $\gamma$ H2AX. Ajuba binding partners include proteins involved in DNA replication and damage, such as SKP2, MCM2, MCM7 and RPA70. Taken together, our data support that Ajuba promotes liver cell proliferation associated with development, regeneration and tumour growth and is involved in DNA replication and damage repair.**

**Keywords:** Ajuba; DNA damage; liver cancer; liver regeneration; proliferation

Cell proliferation is the fundamental process needed for cell renewal, wound repair and tissue regeneration and is dependent on the tightly controlled process of DNA replication [1,2]. However, cell proliferation is increased in malignant cells with the difference between healthy and tumour cell proliferation being the loss of control in malignant cells over the process [3,4]. DNA replication begins at origins of replication (ORI) located throughout the genome and ORI licensing occurs during S-phase of cell cycle when the pre-replication complex is assembled [5]. The pre-replication complex is formed by proteins such as origin recognition complex subunit 1 (ORC), mini-chromosome maintenance (MCM2-7) and cell division cycle 6 (CDC6).

Ajuba is a LIM-domain protein described as an adaptor protein by linking and modulating different

members of functional complexes [6]. Ajuba contains a nuclear export sequence, enabling it to translocate from the cytoplasm to the nucleus and three tandem LIM motifs in its C terminus [7–10]. Ajuba is a versatile scaffold protein associated with numerous protein complexes and among the best characterized function of Ajuba is its role in stabilizing cell–cell junctions by direct binding to F- and  $\alpha$ -tubulin [11,12].

Ajuba has been described to be involved in several proliferation pathways such as the Hippo and Wnt signalling pathways and in the ATR-mediated DNA damage response pathway [13–15]. It has also been found to be dysregulated in cancer [13,16–18]. Ajuba was found to be significantly upregulated in colorectal cancer, oesophageal squamous cell carcinoma and cervical cancer [17,19–21]. However, its reported function in

## Abbreviations

CCl<sub>4</sub>, carbon tetrachloride; CDC6, cell division cycle 6; DEN, diethylnitrosamine; EdU, 5-ethynyl-2'-deoxyuridine; ESCC, oesophageal squamous cell carcinoma; HCC, hepatocellular carcinoma; HUVEC, human umbilical vascular endothelial cells; MCM, mini-chromosome maintenance; ORC, origin recognition complex subunit 1; ORI, origins of replication; PHx, partial hepatectomy; PMA, phorbol 12-myristate 13-acetate; RPA, replication binding protein A; sh, short hairpin.

cancer is contradictory. There are reports which describe Ajuba as a driver of tumour cell proliferation [19–26], whereas in others, it is described as a tumour suppressor and an inhibitor of proliferation [27–29]. Additionally, Ajuba was found to be mutated in cutaneous and oesophageal squamous cell carcinoma (ESCC) [16–18,25,30]. Non-silent Ajuba mutations were found in 3.9% of a 490 ESCC tumour cohort. Tumours with mutations in Ajuba had lower Ajuba expression and significantly better patient survival when compared to tumour samples with non-mutated Ajuba expression [30].

Thus far, the role of Ajuba in liver cancer has been investigated in three publications resulting in contradictory conclusions. Two reports describe Ajuba as a driver of hepatocellular carcinoma (HCC) cell proliferation [6,31], whereas one paper describes Ajuba as a tumour suppressor and inhibitor of cell growth in HCC [28]. We were therefore convinced that elucidating the role and mechanism of how Ajuba is involved in proliferation in the liver in both healthy and regenerating cells and in liver tumour cells is crucial. Therefore, in this study, we investigated the role of Ajuba in HCC and in regenerating liver tissue, focusing on its role in cell proliferation.

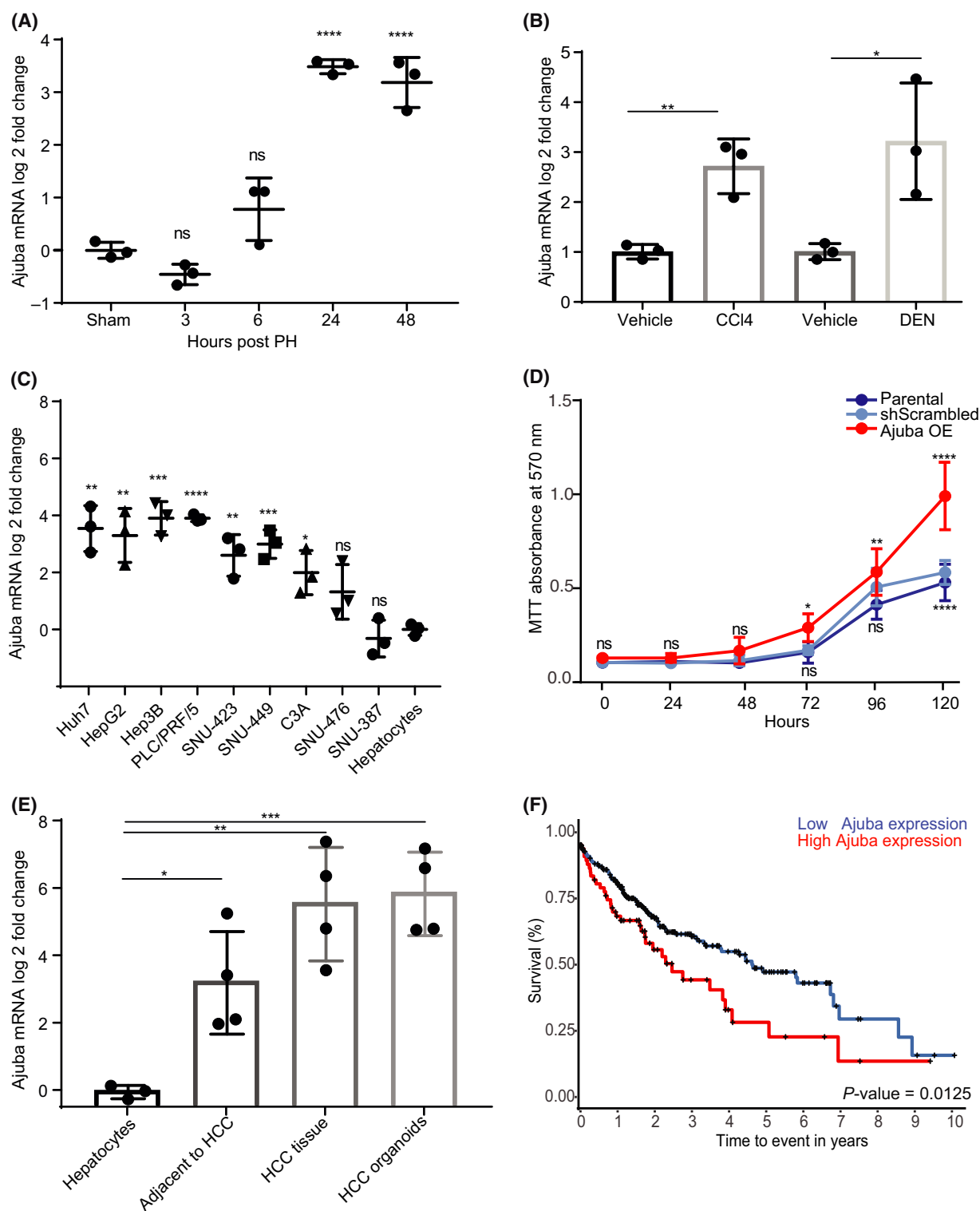
## Results

### Ajuba expression coincides with cell proliferation in normal and malignant liver cells

We first questioned if Ajuba expression is increased when cells transition from a quiescent to a proliferative state using the well-established model of partial hepatectomy (PHx) [1]. Following PHx, liver cells are synchronized to enter cell cycle and replicate to replace the lost tissue. Ajuba mRNA increased 24–48 h following PHx (Fig. 1A). Ajuba protein expression increased and coincided with hepatocyte proliferation [32], occurring 48–72 h post PHx (Fig. S1). Next, we induced regenerative

proliferation by damaging the liver with carbon tetrachloride (CCl<sub>4</sub>) and diethylnitrosamine (DEN) [33,34] and Ajuba mRNA was significantly increased in the damaged liver tissues (Fig. 1B). Ajuba mRNA and protein expression were higher in proliferating malignant liver cancer cell lines when compared to non-proliferating hepatocytes in culture (Fig. 1C and Fig. S2). We next questioned if Ajuba expression is modulated when cells transition from a proliferative to a differentiated or a cell cycle arrested state. The monocyte cell line U937 was differentiated to mature macrophage-like cells with phorbol 12-myristate 13-acetate (PMA) [35,36] or treated with nocodazole to arrest cell growth in the G2 phase of cell cycle [37]. Both conditions blocking cell proliferation resulted in significantly lower Ajuba mRNA levels (Fig. S3). We next used lentiviral transduction of an Ajuba expression construct to demonstrate that Ajuba overexpressed in Huh7 HCC cells leads to an increase in proliferation compared to the parental and shScrambled controls (Fig. 1D). In human livers samples containing HCC tumours, we dissected tumour and adjacent non-tumour tissues and measured an increased expression of Ajuba mRNA compared to normal hepatocytes (Fig. 1E). Also, Ajuba mRNA was highly expressed in human HCC organoids, which were actively proliferating as shown by immunofluorescence of positive 5-ethynyl-2'-deoxyuridine (EdU) incorporation [38] (Fig. 1E and Fig. S4). Furthermore, we consulted The Cancer Genome Atlas [39] and plotted Kaplan–Meyer curves to determine HCC patient survival with high vs. low Ajuba expression. High expression of Ajuba correlated with a decrease in HCC patient survival (Fig. 1F). Taken together, our data demonstrate that Ajuba expression coincides with cell proliferation in both normal and malignant liver tissues and high tumour expression of Ajuba is correlated with decreased HCC patient survival.

**Fig. 1.** Ajuba expression coincides with cell proliferation in normal and liver malignant cells. (A) Ajuba mRNA expression level in liver tissue pre- and at different time points post 70% PHx, statistical test used: one-way ANOVA with Dunnett's multiple-comparison test, error bars show SD,  $n = 3$ . (B) Ajuba mRNA expression level measured by RT-qPCR in mouse livers after either 14-week treatment with CCl<sub>4</sub> (0.5  $\mu\text{L}\cdot\text{g}^{-1}$  of 20% CCl<sub>4</sub>) or 24 h after DEN injection (100  $\text{mg}\cdot\text{kg}^{-1}$ ), olive oil was used as a vehicle, statistical test used: unpaired  $t$ -test, error bars show SD,  $n = 3$ . (C) Ajuba mRNA expression level measured by RT-qPCR liver cancer cell lines and normalized to isolated human hepatocytes, statistical test used:  $t$ -test with multiple-comparison correction Holm–Sidak, error bars show SD,  $n = 3$ . (D) MTT proliferation assay comparing parental, shScrambled and Ajuba OE cell lines. The absorbance was measured at 570 nm 1 h after MTT addition over the span of 5 days. Statistical test used: two-way ANOVA with Tukey's multiple-comparison test, error bars show SD,  $n = 2$ , one representative plot is shown with technical quadruplicates. (E) Ajuba mRNA expression in primary human hepatocytes, human liver tissue isolated from HCC or from tissue adjacent to the HCC tumour tissue and HCC-derived human organoids. Statistical test used: unpaired  $t$ -test, error bars show SD,  $n = 3$ /control and  $n = 4$ /group. (F) Ten-year Kaplan–Meyer survival curves were generated with data from TCGA and used to calculate HCC patient survival according to their Ajuba expression (high = top 20%,  $n = 73$ ) and low expression (low = bottom 80%,  $n = 296$ ), statistics was computed using log-rank test,  $P$ -value = 0.0125. For all analyses, ns denotes  $P > 0.05$ , \* $P < 0.05$ , \*\* $P < 0.01$ , \*\*\* $P < 0.001$  and \*\*\*\* $P < 0.0001$ .



### Loss of Ajuba expression leads to decreased cell proliferation

Based on our observations that proliferating cells were associated with increased Ajuba expression, we wanted

to investigate if Ajuba was necessary for cell proliferation, particularly in physiological processes like liver regeneration and hepatocarcinogenesis. Therefore, we attempted to generate an Ajuba KO mouse line using

CRISPR/CAS9 and pronuclear injection (Fig. S5a–d). However, following extensive breeding and genotyping, we were unable to generate a homozygous Ajuba KO mouse line (Fig. 2A,  $n = 400$ ). We performed timed matings and *in vitro* fertilization to genotype embryos and blastocysts respectively. After again only obtaining WT and heterozygous KO mice, we concluded that the homozygous Ajuba KO mice were embryonically lethal (Fig. S5e–f). This result was supported by our parallel observation that full loss of Ajuba using CRISPR/Cas9 KO in the RIL-175 mouse HCC cell line leads to non-proliferating and non-viable clones [40]. Failing to generate a knockout mouse or cell lines, we switched to study loss of Ajuba expression using lentiviral transduction of short hairpin (sh) RNAs. We modulated Ajuba expression in the human Huh7 cells using two lentiviral constructs targeting a coding (shAjuba1) and non-coding (shAjuba2) region of Ajuba. We observed a significant decrease in Ajuba mRNA and protein compared to the shScrambled control (Fig. 2B and Fig. S6). We next performed several biological assays *in vitro* and *in vivo*. Using an MTT assay to assess cell proliferation, we observed that proliferation was significantly decreased in Huh7 cells with knocked-down Ajuba expression (Fig. 2C). Moreover, Huh7 cells with loss of Ajuba expression had a significantly decreased ability for colony formation (Fig. 2D). The loss of cell growth *in vitro* was also confirmed *in vivo* using the syngeneic tumour model, RIL-175 mouse HCC cells in C57Bl/6 mice. After 11 days, tumour volumes were significantly decreased in cells transduced with the shRNA targeting the coding region of Ajuba (shAjuba1) and a trend of smaller tumours was observed in shAjuba2 shRNA targeting the non-coding region (Fig. 2E and Fig. S7). To give further evidence of the biological importance of Ajuba in normal cells, we assessed the impact of loss of Ajuba expression in human umbilical vascular endothelial cells (HUVEC). In a tube formation assay [41], loss of Ajuba expression decreased total vessel length thereby suggesting its importance in the process of angiogenesis (Fig. 2F). Taken together our data indicate that Ajuba is necessary for proliferation in liver tumour cells, in normal endothelial cells and for embryonic development.

### Ajuba has a nuclear localization in proliferating cells and involved in DNA replication

Supporting a role of Ajuba in proliferation, we could demonstrate by immunohistochemistry the nuclear localization of Ajuba in proliferating HCC tumour and regenerating liver tissues (Fig. 3A). The effect of

altered Ajuba expression on DNA replication and S-phase entry was monitored over a 24-h period. Ajuba KD, OE and control cell lines were synchronized using thymidine, a DNA synthesis inhibitor that arrests cell cycle at the G1/S boundary [42,43]. The arrested cells were then released with complete medium containing 25  $\mu$ M EdU to label the cells entering cell cycle [44]. Ajuba KD cell lines had a significant decreased EdU incorporation and a delay in S-phase entry (Fig. 3B). Delayed S-phase entry is shown by the altered slope of shAjuba1 looking at the y-intercept/2 of the linear regression. The Ajuba overexpressing (OE) cell line, however, showed the highest percentage of EdU incorporation and seem to be the quickest cells to start DNA replication. We next investigated how Ajuba may be involved in proliferation by checking the expression of genes known to be involved in the regulation of cell cycle using the RT2 Qiagen (Garstligweg, Switzerland) microarray composed of cell cycle genes in liver cancer cell line Huh7. In both cell lines with loss of Ajuba expression, we observed reduced expression of genes associated with the initiation of DNA replication, such as S-phase kinase-associated protein 2 (SKP2), MCM2 and MCM3, E2F transcription factor 4 (E2F4) and CDC6 genes (Fig. 3C).

### Ajuba is associated with DNA replication genes

To further understand the mechanistic role of Ajuba in proliferation, we next sought to identify interacting protein partners of Ajuba. We used an Ajuba OE cell line with an HA-tag present in the construct to pull down the Ajuba protein followed by mass spectrometry to identify the proteins binding to Ajuba (Fig. 4A). The Ajuba scrambled control plasmid, containing a scrambled sequence and no HA-tag, was used to account for unspecific binding. We identified 1072 proteins of which 165 proteins were detected uniquely in the Ajuba OE samples (Class I) and 673 proteins that were higher expressed in Ajuba OE compared to the control (log two-fold change) (Fig. 4B,C). Figure S8A displays a string analysis of proteins detected by mass spectrometry that were uniquely or preferentially present in Ajuba OE samples. Several of previously known interaction partners of Ajuba as listed on BioGRID [45], such as large tumour suppressor kinase 1 (LATS1), tyrosine 3-monooxygenase/tryptophan 5-monooxygenase activation protein zeta (YWHAZ) and aurora kinase B (AURKB), as well as new potential interaction partners were found. Using the proteins displayed in Fig. S8B, a Metascape pathway enrichment analysis was performed and among those identified, several pathways in which Ajuba is known to be

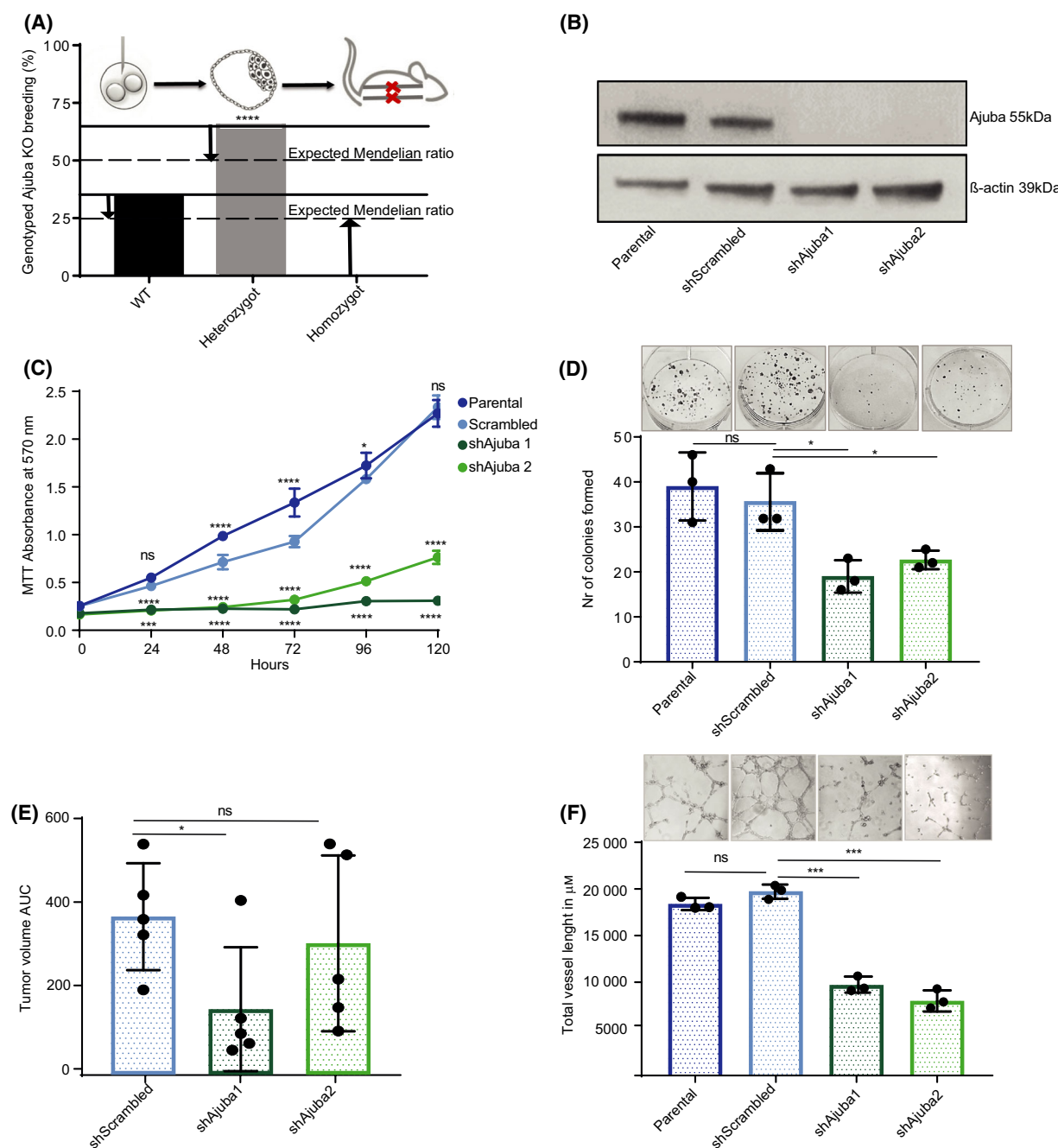
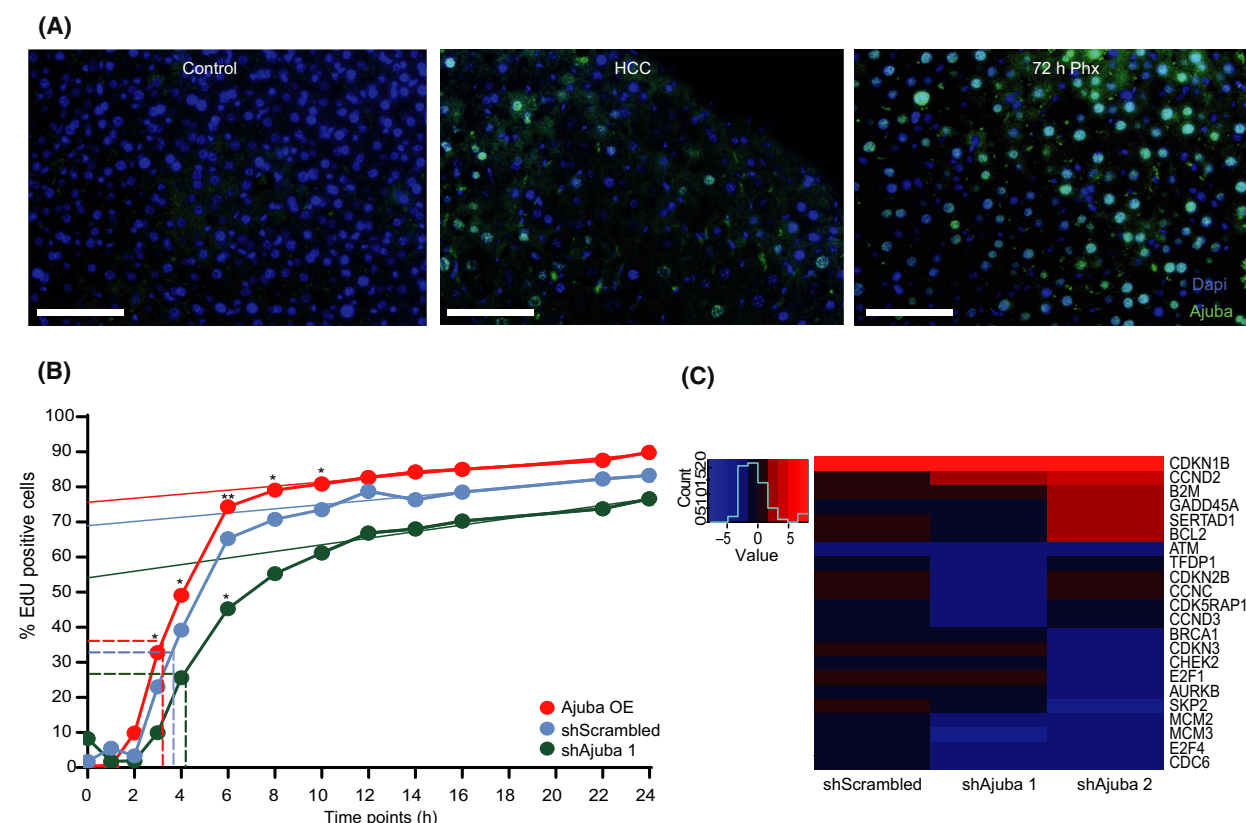


**Fig. 2.** Decreased Ajuba expression leads to decreased cell proliferation. (A) Percentage of Ajuba  $-/-$ , Ajuba  $+/-$  and WT mice after genotyping  $F_2$  generation of Ajuba KO founder lines 1&2 mice ( $N = 400$ , generated by CRISPR/Cas9 Technology). Expected Mendelian ratios for monohybrid cross 1 : 2 : 1 (25% WT, 50% heterozygous and 25% homozygous KO) are depicted as a reference in a dashed line, chi-squared goodness-of-fit test was performed comparing found genotypes with expected Mendelian ratios,  $P$ -value  $< 2.2 \times 10^{-16}$ . (B) Ajuba protein expression in Huh7 cell line with Ajuba KD. (C) Proliferation assay measuring the absorbance at 570 nm 1 h after addition of MTT over the span of 5 days. Statistical test used: two-way ANOVA with Tukey's multiple-comparison test, error bars show SD,  $n = 3$ , one representative plot is shown with technical triplicates. (D) Colony formation assay in Huh7 cell lines in a six-well plate and letting the cells proliferate for 7 days as well as the representative picture of the six-well plate after crystal violet staining, statistical test used: unpaired  $t$ -test, error bars show SD, in triplicates. (E) Graph displaying the area under the curve from the tumour volumes of a subcutaneous syngeneic tumours (RIL-175 cell) in BL/6 WT mice, statistical test used: unpaired  $t$ -test, error bars show SD,  $n = 5$ . (F) Vascular tube formation assay in primary endothelial HUVEC and a representative bright-field pictures (5x), statistical test used: unpaired  $t$ -test, error bars show SD, in triplicate. For all analyses, ns denotes  $P > 0.05$ , \* $P < 0.05$ , \*\* $P < 0.01$ , \*\*\* $P < 0.001$  and \*\*\*\* $P < 0.0001$ .





involved, such as the Hippo pathway, apoptosis and tight junctions, were present [7,10,12,23,46]. Additionally, we found potential binding partners of Ajuba to be involved in cell cycle regulation, G2/M checkpoint, Chk1-mediated inactivation of cyclin B and response to DNA damage (Fig. 4D). We also detected the presence of several proteins involved in translation initiation, RNA splicing and stability as well as transport. Interestingly, potential binding partners were found in various cellular compartments such as the cell–cell junctions, cytoplasm, nuclear as well as mitochondrion and ribosome (Fig. S9). Looking at the pathway enrichment of Class I and Class II separately, proteins involved in protein localization to nucleus and synthesis of DNA and DNA translation pathways as well as S-phase and cell cycle checkpoints and Chk1/Chk2-mediated response were present (Fig. S10). To validate our findings that Ajuba has a direct interaction with proteins involved in cell cycle, DNA replication and

DNA damage, we performed immunoprecipitation experiment and could demonstrate that Ajuba binding partner include replication binding protein A (RPA) subunit 70 (RPA70), SKP2, MCM2 and MCM7 (Fig. 4E).

### Ajuba depletion leads to increased DNA damage expression

As several potential interaction partners of Ajuba were found to be involved in pathways involved in the DNA damage response, we questioned if defects in proliferation are due to an increase in DNA damage with a loss of Ajuba expression. We observed an increase in DNA damage in cells with loss of Ajuba expression already at the steady-state level as shown by the increase in the DNA damage marker  $\gamma$ H2AX by immunocytochemistry (Fig. 5A), FACS (Fig. 5B) and immunoblot (Fig. 5C). Coinciding with  $\gamma$ H2AX,

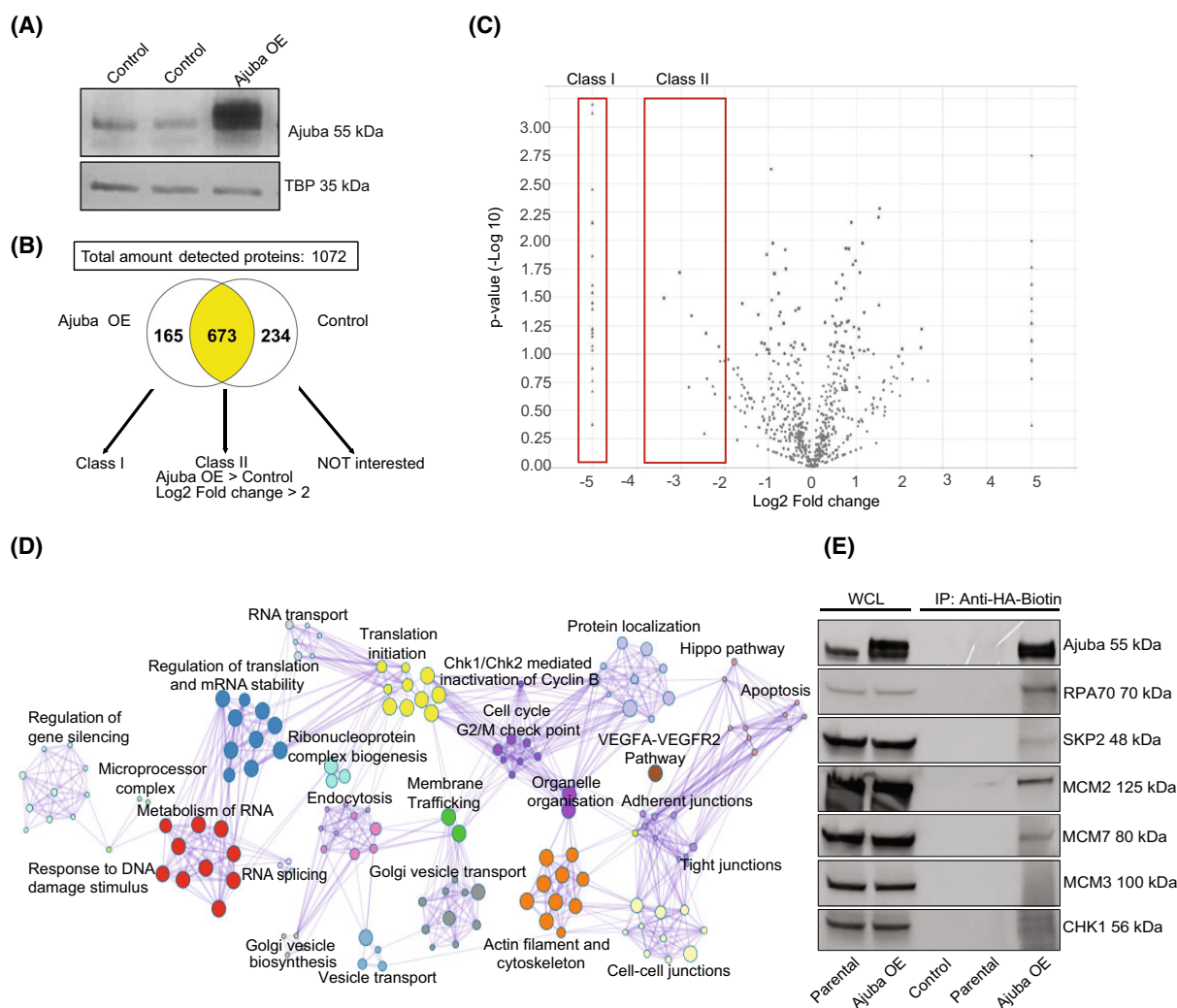


**Fig. 4.** Ajuba is associated with DNA replication genes. (A) Ajuba protein expression of Ajuba OE Huh7 cell line using lentiviral transduction. (B) Venn diagram displaying the total number of proteins identified by Mass spectrometry. The following settings were used: protein 1.0% False discovery rate (FDR). Minimum 2 peptides and 0.1% peptide FDR. Selection criteria for Class I and Class II proteins (>2 log-two fold change) is displayed. Huh7 cell lines with Ajuba OE containing an HA-tag and scrambled control cell line without HA-tag were used. (C) Volcano plot of all proteins detected. (D) Pathway enrichment analysis of binding partners (Classes I and II) of Ajuba using Metascape found after immunoprecipitation of Ajuba OE cells using HA tag. (E) Immunoprecipitation and western blot analysis of Huh77 Ajuba OE and parental cell lysate. Protein A or G agarose/Sepharose beads were used as control. Cell lysates were incubated overnight with anti-HA-Biotin ab.

we detected an increase in RPA70 which binds to single-stranded DNA and sites of DNA damage [47,48] (Fig. 5D). The loss of Ajuba also resulted in the cells being significantly more sensitive to DNA damage induced by irradiation (Fig. 5E). Sensitivity to irradiation was tested by irradiating the cell lines at different dosages ranging from 0 to 6 gray and measuring recovery by colony formation to determine the percentage of survival (Fig. S11). Lastly, we tested the efficiency of DNA damage repair and compared the percentage of DNA repair occurring between two time points, 2 and 4 h post irradiation. The scrambled

control cells showed the highest percentage of DNA damage repair, whereas both cell lines with loss of Ajuba expression displayed a lower DNA damage repair from 2 to 4 h post irradiation (Fig. 5F and Fig. S12A).

## Discussion

In previous publications, Ajuba has been linked to proliferation; however, its role was unclear as it was described as both a driver [19–26] and inhibitor of cell proliferation [27–29]. In our study, we provide

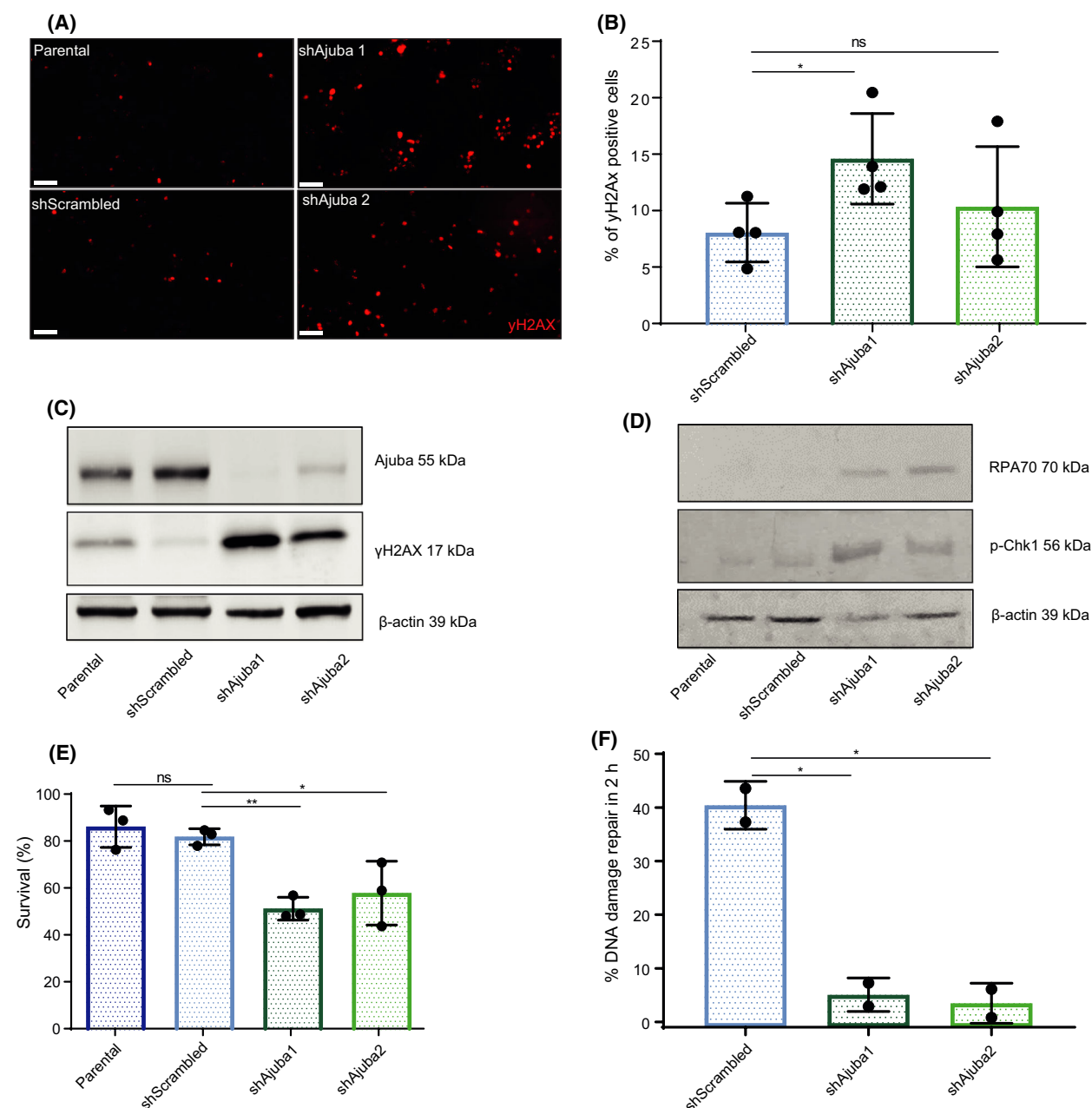


**Fig. 5.** Ajuba depletion leads to increased DNA damage expression. (A) Immunofluorescent pictures of Huh7 cell lines staining for γH2Ax. White bar represents 100 μm. (B) Percentage of γH2Ax positive cells assessed using FACS analysis and a DNA Damage Staining kit (FlowCollect™); statistical test used: unpaired t-test, error bars show SD,  $n = 4$ . (C) Protein expression of γH2Ax assessed by western blot in Huh7 cell lines with Ajuba KD. β-actin was used as a loading control. (D) Western blot analysis of Huh7 cell lines with Ajuba KD stained for RPA70 and p-Chk1. β-actin was used as a loading control. (E) Percentage of colonies that survived after a 3 gray irradiation in Huh7 cell lines, statistical test used: unpaired t-test, error bars show SD, in triplicate. The colonies were stained with crystal violet and counted with ColCounter. Statistics was computed with GraphPad using non-irradiated cells as a measure of 100%. (F) Percentage of DNA damage repair that occurred between 2 and 4 h after a 2 gray irradiation. FACS analysis was used to compute the percentage of γH2Ax positive cells 2 and 4 h. To compute the percentage of repair, 2 h time point was considered as 100% damage, statistical test used: unpaired t-test, error bars show SD,  $n = 2$ . For all analyses, ns denotes  $P > 0.05$ , \* $P < 0.05$ , \*\* $P < 0.01$ , \*\*\* $P < 0.001$  and \*\*\*\* $P < 0.0001$ .



convincing evidence that particularly in liver cells, Ajuba is important in proliferation in both malignant and normal cells and tissues. We found Ajuba to be significantly increased in actively proliferating normal and malignant liver cells and tissues. It was significantly upregulated in hepatocyte compensatory proliferation in models of PHx and during damage repair response following damage due to toxin exposure. Ajuba was also found to be significantly more expressed in proliferating liver cancer cells, as well as in human HCC tumours and HCC organoids. Moreover, when monocytic cells switch from a proliferative to a differentiated state, Ajuba expression was reduced. Previous data from our lab demonstrated that knockout of Ajuba using CRISPR/Cas9 resulted in non-viable HCC cell lines [40]. This observation, together with the embryonic lethality of CRISPR/Cas9 KO animals has also been supported by Loganathan et al. [49], and that Ajuba expression was found during embryogenesis in all embryonic germ layers and within fetal components of the developing placenta [50,51]. However, these findings contradict the report in which Ajuba KO mice were reported to have a mild phenotype [52].

Since CRISPR/Cas9 KO of Ajuba led to non-viable clones, we chose to study Ajuba function using lentiviral transduction of shRNAs to knockdown its expression. With loss of Ajuba expression, we observed that the proliferation rate of HCC tumour cells was decreased *in vitro*, and syngeneic tumours had smaller volumes *in vivo*. With publicly available data from The Cancer Genome Atlas, we found a correlation of high Ajuba expression with poor HCC patient survival, which support the data of Zhang et al. [6], showing that Ajuba expression is related to a more aggressive malignancy and adverse clinical outcome.

We found that cells with loss of Ajuba expression have lower levels of *SKP2*, *MCM2*, *MCM3*, *E2F4* and *CDC6*, all genes involved in the initiation of DNA replication. To provide further evidence that Ajuba could be involved directly in the DNA replication complexes, we identified direct interaction partners by MS and co-IP using an Ajuba OE cell line. We identified that several potential binding partners of Ajuba were found to be involved in DNA replication and cell cycle control and checkpoints, all pathways with proteins localized in the nucleus. We could confirm that Ajuba is indeed expressed in the nuclear compartment proliferating cells and tissues [7,53], which is also supported by studies showing that Ajuba can be translocated between the cytoplasm and the nucleus [10].

Several of the genes found to be differentially expressed after Ajuba KD as well as proteins identified as potential interaction partners of Ajuba seemed to be involved in

DNA replication and more precisely to the pre-replication complex. We therefore decided to take a closer look at the very beginning of DNA replication during the S-phase of cell cycle by assessing if the S-phase entry of the cells with loss of Ajuba expression is affected. We found Ajuba KD cells to have not only a less efficient DNA replication as shown by the decreased percentages of cells being positive for EdU but also a delay of S-phase entry. This could be because the Ajuba-depleted cells had less *SKP2*, *MCM2*, *MCM3* and *CDC6* and therefore had problems efficiently licensing the ORI leading to less efficient DNA replication. A reduction in some MCM proteins in human cancer cells causes a rapid increase in the level of DNA damage under normal conditions of cell proliferation and a loss of viability when the cells are subjected to replication interference [54]. Our data show that with decreased Ajuba expression we also have a decrease in proliferation as well as decreased levels of MCM proteins. We therefore investigated if loss of Ajuba leads to an increase in DNA damage.

In the pathway enrichment analysis of potential Ajuba binding partners, cell cycle checkpoints, response to DNA damage and Chk1-mediated responses were among the pathways that were found. Additionally,  $\gamma$ H2AX as a measure of DNA damage was observed in Ajuba-depleted cells indicating that there was an increase in the baseline levels of DNA damage. Moreover, the increased expression of RPA70 which binds to ssDNA and sites of DNA damage binding [47,48,55] gave us a further indication of Ajuba being involved in DNA replication and damage. Supporting our data, Fowler et al. and Kalan et al. described RPA70 as a direct interaction partner of Ajuba and that Ajuba binding to RPA70 inhibits induction of ATR [15,56]. In addition to Ajuba KD cell lines expressing increased levels of  $\gamma$ H2AX, they were more sensitive and appeared less able to initiate the DNA repair program in response to irradiation-induced DNA damage. Furthermore, we found Ajuba-depleted cells to also express more p-Chk1, which is occurring in the presence of DNA damage and leads to cell cycle arrest [57].

In summary, our study provides evidence that Ajuba supports liver cell proliferation associated with development, regeneration and tumour growth, which may be attributed to its association with DNA replication and repair proteins.

## Materials and methods

### Partial hepatectomy model

Mice underwent a standard hepatectomy resecting two thirds of the liver according to previously described protocol [32].

The mice used in this study were 6- to 8-week-old (~20 g) female C57BL/6JRccHsd provided by Harlan, the Netherlands. Animals were kept in a temperature-controlled room with a 12 h dark/light cycle. Experiments were done with Institutional Animal Care and Use Committee approval and in strict accord with good animal practice as defined by the Office of Laboratory Animal Welfare. Littermates were randomly assigned to control sham or partial hepatectomy groups. For analgesia, 0.05 mg·kg<sup>-1</sup> buprenorphine (Temgesic, Indivior Schweiz AG, Baar, Switzerland; Swissmedic Cat. No. 41931) was injected subcutaneously prior to surgery. During surgery, which lasted 20–25 min, mice were anesthetized by isoflurane inhalation. The mice were immobilized in a supine position and the liver exposed by transverse laparotomy. Following laparotomy, Vicryl 4.0 suture (Ethicon, Baar, Switzerland; VCP496) was used to ligate the left and median liver lobes. The ligated liver lobes were then resected using surgical scissors. The peritoneal cavity was irrigated with saline solution and the abdomen closed using a two-layer running suture. Liver tissue from sham-operated mice were used as non-regenerating control. In sham-operated mice, a laparotomy was performed, the liver was manipulated with a cotton-coated stick, irrigated with saline solution and the abdomen was sutured closed. After PHx livers were allowed to regenerate for various time points up to 7 days. At experimental end points, mice were anesthetized by isoflurane inhalation. Blood was collected *via* the vena cava and centrifuged for serum. Mice were sacrificed by exsanguination. Liver was carefully excised, and tissues were cut in 3 × 3 mm pieces, frozen in liquid nitrogen and stored at -80 °C or fixed in 4% formalin overnight at room temperature.

### ***In vivo* CCl<sub>4</sub> and DEN liver injury models**

C57BL/6 mice were treated for 14 weeks with carbon tetrachloride (CCl<sub>4</sub>) in order to induce hepatotoxicity and fibrosis development [33,58]. CCl<sub>4</sub> was injected intraperitoneally twice a week using 0.5 µl·g<sup>-1</sup> of 20% CCl<sub>4</sub> diluted in olive oil. Control mice were injected with the same volume of olive oil. Diethylnitrosamine (DEN) injection was used to induce an acute-phase hepatotoxicity and provoke compensatory regeneration. DEN was injected intraperitoneally at a concentration of 100 mg·kg<sup>-1</sup> and liver tissue was harvested 24 h post DEN injection.

### **Cell lines and primary human endothelial and hepatocyte cultures**

All human liver cancer cell lines were purchased from American Type Culture Collection [ATCC (Huh7, HepG2, Hep3B, skHep1, C3A, PLC/PRF/5, SNU-387, SNU-423, SNU-449, SNU476, HLE and HLF)] and cultured either in Dulbecco's Modified Eagle's or RPMI medium 1640 (Life Technology, Zug, Switzerland) with 10% of FBS,

100 U·mL<sup>-1</sup> penicillin and 100 µg·mL<sup>-1</sup> streptomycin (Life Technology). Note that skHep1 is of endothelial origin as reported by several publications and should be considered with care [59–61]. Only Huh7 cell line was cultured in RPMI medium GlutaMax with 10% FBS and 100 µg·mL<sup>-1</sup> penicillin/streptomycin (Life Technology). All lines have been tested and are negative for mycoplasma contamination using PCR Mycoplasma Test Kit (Promokine, Vienna, Austria). Primary human endothelial cells (HUVEC) were isolated from umbilical cord and cultured in MCDB 131 medium with 5% of FBS, 10 ng·mL<sup>-1</sup> of HEGF (Sigma-Aldrich, Buchs, Switzerland), 1 ng·mL<sup>-1</sup> of hydrocortisone (Sigma-Aldrich) and antibiotics.

Primary human hepatocytes were isolated from consented patients at the University Hospital of Bern undergoing surgical liver resection. Informed consent was obtained prior to surgery in compliance with the local ethics regulations and under approval of local ethics commission. Hepatocytes were cultured according to an established standard procedure [62] and seeded on collagen-coated plastic dishes prior to culture in Dulbecco's minimum essential medium (DMEM) supplemented with 10% fetal bovine serum, 50 U·mL<sup>-1</sup> penicillin, 50 µg·mL<sup>-1</sup> streptomycin and 1 µmol·L<sup>-1</sup> dexamethasone. After overnight culture, the medium was replaced by serum-free Williams E medium<sup>®</sup>glutaMax<sup>™</sup>.

### **Monocyte differentiation using PMA**

Human monocyte cell line U-937 was purchased from American Type Culture Collection (ATCC) and cultured in RPMI-1640 medium. U-937 differentiation was induced using PMA as previously described in literature [35,36]. U-937 cells were treated for 3 days with PMA, Nocodazole, DMSO or left untreated. PMA (160 nM dissolved in DMSO) to induce differentiation into less proliferative macrophages. Nocodazole treatment (100 ng·mL<sup>-1</sup> dissolved in DMSO) was used as a positive control for growth arrest and DMSO only as a solvent control. Bright-field microscopy was used to take pictures at day 1 and day 3 after the treatments to show differences in cell number and cell morphology (differentiation status). After 3 days, cells were harvested and RNA extracted using Triazol (Thermo fisher, Basel, Switzerland) and further processed for qPCR analysis to detect Ajuba mRNA levels.

### **Ajuba overexpression using lentiviral transduction**

Liver cancer cell line Huh7 was transduced with a lentiviral Ajuba expressing construct as previously described [40]. The Ajuba plasmid was purchased from Harvard, Boston, MA, USA; PlasmID:Phage\_CMV\_C\_FLAG\_HA\_IRES\_PURO.

All experiments were carried out on cells at 25–50% confluence and the efficiency of the transduction was assessed by real-time qPCR and immunoblot.

### Cell Proliferation assay (MTT assay)

Cells were seeded in a 96-well plate at a density of 2000 cells per well in 200  $\mu$ L of medium. Cells were incubated for 6 h to adhere to the plate. Every day at the same time, MTT (5 mg of thiazolyl blue dissolved in 5 mL DMEM) was added in one tenth of the culture volume (20  $\mu$ L for 200  $\mu$ m plated) in each well (four wells per time point and condition) and incubated for 1 h. Then, the medium was discarded and replaced by 200  $\mu$ L of DMSO. Using the Tecan Infinite 2000, the plate was shaken and read at an absorbance of 570 nm.

### HCC patient-derived organoids cultures

Human HCC tumour tissues were obtained from consented patients at the University Hospital of Bern undergoing surgical liver resection. Informed consent was obtained prior to surgery in compliance with the local ethics regulations and under approval of local ethics commission. HCC tissue as well as adjacent to HCC tissue were used for qPCR analysis. Tumour samples were taken from within the tumor margin as well as from outside the tumor margin to be used as a non-malignant control. Tumour tissue was mechanically disrupted and enzymatically digested to obtain 3D organoids culture as previously described [63]. Briefly, tumours were collected in basis medium and mechanically disrupted, and then dissociated using collagenase type II enzyme mix. Tumour was digested for 1 h at 37 °C mixing the samples every 20 min. Then, the samples were filtered (100  $\mu$ m) and erythrocytes lysed using EC lysis buffer. Finally, single-cell suspension was achieved using incubation in Accutase™. The single-cell suspension was then filtered again (40  $\mu$ m) and re-suspended in Matrigel. Drops of Matrigel and single-cell suspension were added in a 24-well plate and dried for 30 min at 37 °C. Finally, special supplemented medium was added to the Matrigel drops and organoids were left several days to form HCC organoids. Human organoids were kept in culture up to several weeks at 37 °C in a humidified incubator with 5% of CO<sub>2</sub>.

### Public data acquisition

On the 4th of September 2021, HCC RNA-seq expression (counts) and survival data of liver cancer were downloaded from The Cancer Genome Atlas [39].

### Survival analysis

The survival curves were calculated with the R function `survfit` from the R package `survival` [64] with the formula `Surv(time,vitalstatus)~categorie` and plotted with the R function `ggkm` from the R package `ggkm` [65]. The samples labelled as 'primary tumor' were included. The data were separated in high expression (top 20%) and low expression

(bottom 80%). Using interactive tools on publicly available data visualization tools such as the Human Protein Atlas, the effect of different cut-off threshold can also be tested. Two samples were discarded due to missing information.

### Generation of Ajuba KO mice

Ajuba KO mice were generated using clustered regularly interspaced short palindromic repeats (CRISPR/Cas9) technique and subsequent pronuclear injection. All animal experiments were performed according to the regulations drafted by the Association for Assessment and Accreditation of Laboratory Animal Care. Ajuba KO mice were created in collaboration with the Theodore Kocher Institute Bern (TKI). Recombinant Cas9 nuclease, tracrRNA, crRNA and nuclease-free duplex buffer were purchased from IDT. We used two gRNA-targeting mouse Ajuba gene creating a 693 kDa deletion in Exon 1. Ajuba mouse protein contains eight exons and no alternative splice variants. Target sites corresponding to the targeting sgRNA were predicted by the web-based tool (<http://crispr.mit.edu>). Predicted the cleavage sites and considered them as a potential off-target event. The specifically designed CRISPR/Cas9 riboprotein complex was microinjected into wild-type zygotes (C57BL/6J) as described by Aida et al. [66]. In short, crRNAs were mixed separately with the tracrRNA and incubated at 95 °C for 2 min; the tubes were let to cool down at room temperature for at least 15 min. Shortly before injection the crRNA-tracrRNA duplexes were mixed with EmbryoMax buffer at room temperature. Finally, the Cas9 protein was added and mixed with the riboprotein complex at 37 °C for 20 min before being centrifuged at 18 000 *g* for 10 min at 4 °C. The CRISPR/Cas9 riboprotein complex was then microinjected into the male pronucleus of previously fertilized and isolated oocytes. Fertilized oocytes were obtained from superovulating young (4- to 6-week-old). After overnight incubation at 37 °C, the oocytes that successfully developed into two cell stage zygotes were transferred into the oviductal ampullae of pseudo-pregnant females using standard protocols (10–15 zygotes per oviduct). We have conducted two separate rounds of pronuclear injections. In the first series of injections, we transplanted 90+ two-cell embryos into six recipient mice of which eight pups were born. Five of these eight mice survived and they were further analysed. The second series of injections yielded 56 two-cell stage embryos, which were transferred to four mice and of which two mice survived. The resulting founder mice were genotyped by PCR. Founders were backcrossed with C57BL/6J and mutated alleles in F<sub>1</sub> mice were identified by DNA sequencing (Fig. S5). F<sub>1</sub> mice with identical mutations were intercrossed to generate Ajuba KO  $-/-$  mice. F<sub>2</sub> progeny of two distinct Ajuba founder lines was genotyped and used to calculate the generated Mendelian ratio of WT, heterozygous and homozygous mice (Fig. S5). All the generated mice were

genotyped using ear biopsies and our previously designed primers. Primers were designed using the web tool from National Center for Biotechnology Information (NIH) Primer-BLAST tool for specific primer design [67]. Primer Nr1 was designed to differentiate the genotype of the mice according of the total length of the PCR product. From the size of the PCR product we could assess the size of the deletion (WT expected size = 1400 and KO = 700). The PCR products were extracted from the agar gel and sent for sanger sequencing. Analysis of the sequencing was performed using GeneCoder and CodonCode aligner. The sequencing results were used to design specific and unique primers for the different founder lines, targeting the newly created sequence at the deleted regions. Finally, we designed additional primers to determine if mice contain WT sequence by targeting a region found to be absent in all founder lines. Product specifications: Alt-R CRISPR-Cas9 TracrRNA; Alt-R S.p Cas9 hifi nuclease 3NLS (in glycerol); Alt-R CRISPR-Cas9 crRNA 1 (Cas9.Ajuba.1 sequence: CCCGGACGACACTCGGTTAC /PAM = AGG); Alt-R CRISPR-Cas9 crRNA 2 (Cas9.Ajuba.2 sequence: TGGGCTACGACCAGCGCCAC /PAM = GGG) and EmbryoMax buffer (Millipore, Schaffhausen, Switzerland).

### PCR genotyping protocol

The biopsies were collected from all mice and lysed using direct PCR (Viagen Biotech, Basel, Switzerland) following manufacturers protocol. Shortly, 200 µL of lysis buffer mixed with 10% proteinase K (Qiagen) was added to the biopsies and incubated at 55 °C on a shaker overnight. On the next day, proteinase K is inactivated for 20 min at 95 °C. GoTaq 2X PCR master mix (Promega, Dübendorf, Switzerland) was used with the genotyping primer pairs. All PCR conditions were as follows: 95 °C, 2 min; [95 °C, 30 s; 58 °C, 30 s; and 72 °C, 45 s] × 32; 72 °C, 5 min; 4 °C forever. PCR products were run on 3% agarose gels in 1X TAE buffer. After genotyping, the gel bands were cut out and DNA isolated and send for sequencing (Microsynth AG, Balgach, Switzerland) to determine the exact sequence of the mutation. To assess if the homozygous and heterozygous mice were following the expected Mendelian ratios for monohybrid cross 1 : 2 : 1 (25% WT, 50% heterozygous and 25% homozygous KO), we performed chi-square goodness-of-fit test. We therefore use the R function `chisq.test`, comparing the actual and expected nr of genotyped mice.

### Lentiviral transduction

Liver cancer cell line Huh7 was transduced with two shRNAs targeting Ajuba and one lentiviral Ajuba expression construct as mentioned above and previously described [40]. The shRNAs were purchased from MISSION™,

Sigma-Aldrich. Clone shAjuba1 (NM-032876.4-1385s1c1) is targeting a coding region and clone shAjuba2 (NM-032876.4-2786s1c1.) is targeting a non-coding region of Ajuba.

Lentiviral scrambled control shRNA with random sequence Clone shScrambled MISSION® pLKO.1-puro non-mammalian shRNA Control Plasmid. Ajuba expression construct: Clone Ajuba OE Harvard PlasmID:Phage\_CMV\_C\_FLAG\_HA\_IRES\_PURO. All experiments were carried out on cells at 25–50% confluence and the efficiency of the transduction was assessed by real-time qPCR and immunoblot.

### Western blot

Total protein extraction was performed using RIPA cell lysis buffer (10 mM Tris with pH 8, 1 mM EDTA pH 8, 150 mM NaCl, 0.5% NP40) with addition of protease inhibitors (1 mM NaF, 10 mM NaVO<sub>3</sub>, 1 mM PMSD, 1X protease inhibitor cocktail – Sigma P1860). The cell lysates were sonicated (Sonopuls, Bandelin), then centrifuged and only the supernatant was kept for further analysis. Snap-frozen tissue pieces were dissociated using a TissueLyser (Qiagen) for 2 min at 20 Hz in RIPA buffer. The protein lysate concentrations were determined with the Bio-Rad Protein Assay System (Bio-Rad) as described by the manufacturer. Equal amounts of proteins were separated by SDS-PAGE and transferred onto a nitrocellulose membrane using the iBlot2 Gel transfer device. The membrane then was blocked in 5% non-fat dry milk dissolved in PBS for 1h followed by incubation with the primary antibody overnight at 4 °C. After incubation with the HRP conjugated secondary antibody, chemiluminescent reaction was performed with Western Lightning Plus-ECL from Perkin Elmer. Membranes were developed using the X-ray film processor Curix 60 (AGFA). The band size was estimated using Page Ruler™ Prestained Protein Ladder (Fermentas, Basel, Switzerland) and Precision Plus Protein™ DUAL Color Standards (Bio-Rad, #161-0374). Primary antibodies used were rabbit monoclonal anti-Ajuba (1 : 1000 dilution, Cell Signalling, Allschwil, Switzerland), γH2Ax [1 : 1000 dilution, P-Histone H2AX (Ser139), Millipore] and RPA70 (1 : 1000 dilution, Cell Signalling). HRP-conjugated secondary antibodies used were goat anti-rabbit (Dako, Baar, Switzerland). β-actin-HRP (1 : 100 000 dilution, Sigma) as well as antibody against TATA box binding protein (anti-TBP) (1 : 1000 dilution, Cell Signalling) were used as a loading control.

### Quantitative real-time reverse transcription PCR

Total RNA was isolated from human samples and cell lines using Triazole (Thermo Fisher) according to manufacturer's protocol. The quality and concentration of RNA were measured using Nanodrop 2000 Spectrophotometer



(Thermo Scientific). Five-hundred nanogram of total RNA was used for cDNA synthesis using Omniscript RT Kit 200 (Qiagen). mRNA was analysed by quantitative RT-PCR with TaqMan gene expression assays and reagents according to the standard protocols (Applied Biosystem, Muttenz, Switzerland), using specific primers and housekeeping genes 18S FAM as control. We used the TaqMAN ViiA TM 7 Real-Time PCR system from Applied BioSystems for the amplification steps and data collection. Log two-fold changes were computed using the  $\Delta\Delta C_t$  method.  $C_t$  values of target genes (TG) were calculated relative to a reference gene (RG, 18S) using the following formula:  $\Delta C_{tTG} = C_{tTG} - C_{tRG}$ . Experimental groups (TG) are normalized to control group (CG):  $\Delta\Delta C_t = \Delta C_{tTG} - \Delta C_{tCG}$ , and fold increase =  $2^{-\Delta\Delta C_t}$ .

### Colony formation assay

Colony formation assay was performed as previously described [68]. Briefly, 1000 cells per well were plated in triplicate into six-well plates and incubated for 7 days. To stop the colony formation, the medium was removed, and cells were washed twice with DPBS before being dried. Crystal violet was used to stain the cells (3 g crystal violet, 99.9 mL methanol and 49.9 mL acetic acid) by incubating each well for 30 min at room temperature. The number of colonies was counted using the Colcount (Oxford Optromix, Abingdon, UK).

### In vivo syngeneic tumour model

RIL-175 cells were previously transfected with lentivirus to KD Ajuba, and shScrambled control were used to inject subcutaneously on the flank of C57BL/6J mice. Protocol was adapted from Brown et al. [69]; in short,  $1 \times 10^6$  cells were injected,  $N = 5$  mice per condition were used and tumour was measured ever second day using a digital caliper under isoflurane. Tumour volume was calculated according to the modified ellipsoid formula volume =  $(4/3) \times \pi \times (\text{length}/2) \times (\text{width}/2) \times (\text{height}/2)$  [70]. Mice were harvested 2 weeks after injection and tumours carefully excised and snap frozen or paraformaldehyde preserved for further analysis.

### Angiogenesis tube formation assay in 3D Matrigel

Primary endothelial cells were isolated from the umbilical cord to generate HUVEC. Ajuba was KD using shRNA and then a vascular tube formation assay was performed as previously described [70]. Briefly, 150 000 HUVEC were plated per well in a 96-well plate that was coated with 30  $\mu$ L of Matrigel® (BD Biosciences, Allschwil, Switzerland). Pictures were taken with a Leica camera and afterwards analysed by a semi-automated plug-in for IMAGEJ

software as previously described [41]. All experiments were performed in triplicate.

### Immunofluorescence

Tissue samples were fixed in 4% formaldehyde for 24h then processed and embedded in paraffin. Paraffin blocks were sectioned with Leica Microtome in 6- $\mu$ m-thick slides. Sections were stained using Ajuba antibody (Novus Biologicals, Zug, Switzerland, NBP1-39570, concentration 1 : 50) overnight at 4 °C. The secondary antibody, anti-rabbit Cy3 (Life Technologies, Zug, Switzerland, concentration 1 : 300) was incubated for 2 h in antibody diluent (Dako antibody diluents with background reducing components). Coverslips were mounted with VECTASHIELD Antifade Mounting Medium with DAPI (Vector Laboratories, Zug, Switzerland; H-1500) and fluorescence images were taken using an automated inverted microscope (Leica DMI4000 B).

### Flow cytometry assessment of S-phase entry

Huh7 cell lines with Ajuba KD and OE were synchronized at the G1/S transition of cell cycle using thymidine, an inhibitor of DNA synthesis. EdU integration was used to assess the percentage of cells in S-phase at different time points, over the time course of 24 h. Cell synchronization protocol was adapted and optimized for Huh7 from Macheret et al. [43]. Cells were treated with 2 mM of thymidine for 18 h to synchronize cells at early S-phase of cell cycle (G1/S boundary). After thymidine synchronization, the cells were trypsinized and washed twice in warm medium, then released in warm media containing 25  $\mu$ M EdU for various time points (Invitrogen, Basel, Switzerland; Cat. No. A10044). Cells were collected every 2 h and fixed with 90% methanol overnight as previously described [44]. The cells were prepared for flow cytometry using the Click-it Kit (Invitrogen, Cat. No. C-10420) according to the manufacturer's instructions. The genomic DNA was stained with propidium iodide (Sigma, Cat. No. 81845) in combination with RNase (Roche, Basel, Switzerland; Cat. No. 11119915001). EdU-DNA content profiles were then acquired by flow cytometry (SORP LSR II) to assess the percentage of cells that entered S-phase in each condition at each time point.

### RT2 Microarray and data analysis

Cell cycle RT2 profiler PCR gene arrays were purchased from Qiagen. Total RNA was isolated using Promega Extraction Kit according to manufacturer's instructions (Promega). The quality and concentration of the RNA were measured with the Agilent 2100 BioAnalyzer. High-quality RNA samples (RIN > 9) were then reverse transcribed using the first-strand synthesis kit from Qiagen. The



samples were prepared in duplicate in order to have enough cDNA for the two different array plates. Samples were then loaded to the cell cycle array plate according to manufacturer's instructions. Finally, the data were analysed using the GeneGlobe online web analysis tool provided by Qiagen. After selecting the correct RT2 profiler and the species used in the experiment, the raw data were uploaded into the dataset *via* a previously prepared excel sheet of all the qPCR plates. Using the Sample Manager, control group was defined as the scrambled cell line, whereas the other samples were named groups 1–5. Sample Ct- cut-off was set to 35 for both the arrays. A quality control was performed by the program to check for PCR array reproducibility, reverse transcription control and genomic DNA contamination. Data were normalized to an average of four selected housekeeping genes. For the cell cycle array plate housekeeping genes: B2M, GAPDH, HPRT1 and RPLPO were used, and for the hippo pathway array plate, ACTB B2M, GAPDH and RPLP0 were used. Comparative heat maps and fold change were calculated by determining the ratio of mRNA levels to control values using the  $\Delta C_t$  method ( $2^{-\Delta\Delta C_t}$ ). Data were depicted with a heatmap using R.

### Immunoprecipitation and subsequent mass spectrometry (MS)

Immunoprecipitation was performed using the Pierce MS-compatible magnetic IP kit (streptavidin) from Thermo Scientific. Huh7 cell lines, Ajuba OE containing an HA-tag and shScrambled containing no HA-tag were used, respectively, as a sample and as a control for the experiments. Protein was isolated according to the manufactures' instruction 48h after plating with the slight modification of adding proteinase inhibitors and PMSF to the cell lysis buffer. The protein concentration was measured using Bradford assay, and IP was performed with 1000 ng of protein and 60  $\mu$ L of biotinylated anti-HA antibody ( $100 \mu\text{g}\cdot\text{mL}^{-1}$ ). The cell lysate was incubated overnight with the specific biotinylated ab at 4 °C. The next day, antigen/ab complex to streptavidin magnetic beads was incubated for 2 h at 4 °C and then for 20 min at RT. The samples were run in duplicate and sent to the Functional Genomics Center Zurich, ETH, University of Zurich, where samples were further processed and analysed using LC/MS/MS.

### Immunoprecipitation analysis

Immunoprecipitation was analysed using scaffold4. Protein threshold was set to 1.0% FDR and minimum number of peptides to 2. Peptide threshold 0.1% FDR. Database searches were performed by using the Mascot (Swiss\_Prot, human) search program which identified a total of 1072 proteins. We filtered out the proteins that were uniquely expressed in Ajuba OE and named them Class I. From the

proteins that were detected in both samples, we then filtered out the ones that had a two-fold higher expression of total unique peptide count in OE compared to its control and named them Class II, resulting in a total of 247 proteins. All other proteins were not used for further analysis. The full mass spectrometry report table displaying all the detected proteins is available in Table S1 and the list for all proteins of Class I and Class II is available in Table S2.

### Immunoprecipitation and western blot analysis

Immunoprecipitation was carried out overnight at 4 °C on 800  $\mu$ g of total Huh7 Ajuba OE and Huh7 parental cells lysate with Protein A or G agarose/Sepharose beads (Abcam, Basel, Switzerland; ab193262) and  $5 \mu\text{g}\cdot\text{mL}^{-1}$  of monoclonal anti-HA-Biotin (Roche, 12158167001). Beads were washed four times with PBS/Tween 0.1% to remove unbound proteins. Interacting proteins were detected by western blot using the following antibodies: RPA70 (1 : 1000, Cell Signaling #2198), MCM2 (Cell Signaling #3619), MCM3 (1 : 1000, Cell Signaling #4003), MCM7 (1 : 1000, Cell Signaling #3735), SKP2 (1 : 1000, Cell Signaling #2652) and CHK1 (1 : 1000, Cell Signaling #2360).

### Venn diagram

Venn diagrams were drawn using custom Venn diagrams from Bioinformatics & Evolutionary Genomics web tools [71].

### String visualization

Protein selected (Class I and Class II) from the MS analysis was plotted on string-db.org in order to visualize known interactions with Ajuba protein [41].

### Pathway enrichment analysis

Pathway enrichment analysis was performed using Metascape Gene Annotation & Analysis Resource [72]. We used the proteins selected from the MS analysis of Class I, Class II and the combination of Classes I and II to display pathway enrichment. The top 20 statistically significant families of pathways are displayed.

### Immunocytochemistry

HCC cell lines were grown on glass cover slips in eight plates (50 000 cells per well). Cells were fixed with 4% formaldehyde, permeabilized and blocked in 5% goat serum (DAKO, X0907), 0.3% Triton-X-100 (Sigma-Aldrich) in DPBS and stained with an anti- $\gamma$ H2AX antibody 1:500 dilution (Millipore) and matched with Alexa Fluor® 647 conjugated secondary antibodies diluted 1:1000 (Life Technologies). Nuclei were counterstained with DAPI

(1 : 5000), coverslips were mounted with Vectashield Anti-fade Mounting Medium (Vector Laboratories, H-1000) and fluorescence images were taken using the Panoramic 250 Flash II slide scanner (3DHitech, Budapest, Hungary).

### FACS assessment of DNA damage and DNA damage repair

To assess the DNA damage in Huh7 cell lines where Ajuba was previously KD and OE, we used the FlowCollect™ Histone H2A.X Phosphorylation Assay Kit according to the manufacturer's instructions. To assess the DNA damage repair capacity of the different cell lines, we irradiated the cells with 2 gray using Gammacell 40 (Best Theratronics) and used γH2AX as a readout as previously described [73]. The FACS readout was then performed using the H2A.X Phosphorylation Assay Kit 2 and 4 h after a 2 gray irradiation.

### Sensitivity to irradiation

In six-well plates, cells were plated with a density of 1000 cells in 200 μL medium per well. After letting the cells adhere for 6 h, the plates underwent irradiation in a Gammacell 40 (Best Theratronics) at the following doses: 0, 2, 3, 4, 5, 6 and 8 gray as previously described [40]. Non-irradiated cells were used as a control. The sensitivity after irradiation was assessed by the cells capacity to form colonies as described under colony formation assay.

### Graphs and statistical analysis

R was used for the computation of publicly available RNA-seq data and RT2 microarray experiments, and graphs were displayed using R-package GGPLOT2 [74]. Scaffold4 was used for the analysis of the mass spectrometry data. The graphs and the statistics for the remaining graphs were done by using PRISM (Graphpad Software, San Diego, CA, USA). Statistical tests used are mentioned in the corresponding figure legends. For all analyses, NS denotes  $P > 0.05$ ,  $*P < 0.05$ ,  $**P < 0.01$ ,  $***P < 0.001$  and  $****P < 0.0001$ .

### Acknowledgements

We would like to thank Deborah Krauer, Magali Humbert and Prof Mario Tschan for their help with preparing the lentiviruses; Prof Charaf Benarafa for his advice designing the generation of the Ajuba KO mice; Dr Urban Deutsch and Albert Witt for the production of Ajuba KO mice; Prof Marianna Kruithof-de Julio and Dr Sofia Karkampouna for their support with the HCC organoids; Prof Thomas Kaufmann for providing the DEN-treated mouse liver samples. We thank the Flow Cytometry & Cell Sorting and Live Cell Imaging core facilities of the Department of

Biomedical Research, University of Bern, and the Functional Genomics Center Zurich, ETH, University of Zürich, for their support with the mass spectrometry. We also thank Isabel Büchi and Dana Leuenberger for technical support; Dr Adrian Keogh for critically reading the manuscript and the Aclon Foundation for their generous support of the project. Open Access Funding provided by Universität Bern within the CSAL Agreement.

### Author contributions

Conceptualization: ND, DS; Methodology: ND, JG, DS-T, FAB, FB; Formal Analysis: ND, DS-T; Data Curation: ND, DS-T, FAB, FB, GL; Writing-Original Draft Preparation: ND; Writing-Review & Editing: ND and DS; Supervision: DS; Funding Acquisition: DC, DS. All authors have read and agreed to the published version of the manuscript.

### Data accessibility

The data that support the findings of this study are available in Tables S1 and S2.

### References

- 1 Michalopoulos GK, DeFrances MC. Liver regeneration. *Science*. 1997;276:60–6. <https://doi.org/10.1126/science.276.5309.60>
- 2 Malumbres M, Barbacid M. To cycle or not to cycle: a critical decision in cancer. *Nat Rev Cancer*. 2001;1:222–31. <https://doi.org/10.1038/35106065>
- 3 Branzei D, Foiani M. Maintaining genome stability at the replication fork. *Nat Rev Mol Cell Biol*. 2010;11:208–19. <https://doi.org/10.1038/nrm2852>
- 4 Fragkos M, Ganier O, Coulombe P, Méchali M. DNA replication origin activation in space and time. *Nat Rev Mol Cell Biol*. 2015;16:360–74. <https://doi.org/10.1038/nrm4002>
- 5 Moiseeva T, Hood B, Schamus S, O'Connor MJ, Conrads TP, Bakkenist CJ. ATR kinase inhibition induces unscheduled origin firing through a Cdc7-dependent association between GINS and And-1. *Nat Commun*. 2017;8:1392. <https://doi.org/10.1038/s41467-017-01401-x>
- 6 Zhang C, Wei S, Sun W-P, Teng K, Dai M-M, Wang F-W, et al. Super-enhancer-driven AJUBA is activated by TCF4 and involved in epithelial-mesenchymal transition in the progression of hepatocellular carcinoma. *Theranostics*. 2020;10:9066–82. <https://doi.org/10.7150/thno.45349>
- 7 Goyal RK, Lin P, Kanungo J, Payne AS, Muslin AJ, Longmore GD. Ajuba, a novel LIM protein, interacts with Grb2, augments mitogen-activated protein kinase

- activity in fibroblasts, and promotes meiotic maturation of *Xenopus* oocytes in a Grb2- and Ras-dependent manner. *Mol Cell Biol.* 1999;19:4379–89. <https://doi.org/10.1128/mcb.19.6.4379>
- 8 Srichai MB, Konieczkowski M, Padiyar A, Konieczkowski DJ, Mukherjee A, Hayden PS, et al. A WT1 co-regulator controls podocyte phenotype by shuttling between adhesion structures and nucleus. *J Biol Chem.* 2004;279:14398–408. <https://doi.org/10.1074/jbc.M314155200>
  - 9 Sharp TV, Munoz F, Bourboulia D, Presneau N, Darai E, Wang H-W, et al. LIM domains-containing protein 1 (LIMD1), a tumor suppressor encoded at chromosome 3p21.3, binds pRB and represses E2F-driven transcription. *Proc Natl Acad Sci USA.* 2004;101:16531–6. <https://doi.org/10.1073/pnas.0407123101>
  - 10 Jia H, Peng H, Hou Z. Ajuba: an emerging signal transducer in oncogenesis. *Pharmacol Res.* 2020;151:104546. <https://doi.org/10.1016/j.phrs.2019.104546>
  - 11 Alégot H, Markosian C, Rauskolb C, Yang J, Kirichenko E, Wang YC, et al. Recruitment of Jub by  $\alpha$ -catenin promotes Yki activity and. *J Cell Sci.* 2019;132:jcs222018. <https://doi.org/10.1242/jcs.222018>
  - 12 Marie H, Pratt SJ, Betson M, Eppe H, Kittler JT, Meek L, et al. The LIM protein Ajuba is recruited to cadherin-dependent cell junctions through an association with alpha-catenin. *J Biol Chem.* 2003;278:1220–8. <https://doi.org/10.1074/jbc.M205391200>
  - 13 Chen X, Stauffer S, Chen Y, Dong J. Ajuba phosphorylation by CDK1 promotes cell proliferation and tumorigenesis. *J Biol Chem.* 2016;291:14761–72. <https://doi.org/10.1074/jbc.M116.722751>
  - 14 Haraguchi K, Ohsugi M, Abe Y, Semba K, Akiyama T, Yamamoto T. Ajuba negatively regulates the Wnt signaling pathway by promoting GSK-3 $\beta$ -mediated phosphorylation of beta-catenin. *Oncogene.* 2008;27:274–84. <https://doi.org/10.1038/sj.onc.1210644>
  - 15 Fowler S, Maguin P, Kalan S, Loayza D. LIM protein Ajuba associates with the RPA complex through direct cell cycle-dependent interaction with the RPA70 subunit. *Sci Rep.* 2018;8:9536. <https://doi.org/10.1038/s41598-018-27919-8>
  - 16 Gao Y-B, Chen Z-L, Li J-G, Hu X-D, Shi X-J, Sun Z-M, et al. Genetic landscape of esophageal squamous cell carcinoma. *Nat Genet.* 2014;46:1097–102. <https://doi.org/10.1038/ng.3076>
  - 17 Zhang L, Zhou Y, Cheng C, Cui H, Cheng L, Kong P, et al. Genomic analyses reveal mutational signatures and frequently altered genes in esophageal squamous cell carcinoma. *Am J Hum Genet.* 2015;96:597–611. <https://doi.org/10.1016/j.ajhg.2015.02.017>
  - 18 Pickering CR, Zhou JH, Lee JJ, Drummond JA, Peng SA, Saade RE, et al. Mutational landscape of aggressive cutaneous squamous cell carcinoma. *Clin Cancer Res.* 2014;20:6582–92. <https://doi.org/10.1158/1078-0432.CCR-14-1768>
  - 19 Shi X, Chen Z, Hu X, Luo M, Sun Z, Li J, et al. AJUBA promotes the migration and invasion of esophageal squamous cell carcinoma cells through upregulation of MMP10 and MMP13 expression. *Oncotarget.* 2016;7:36407–18. <https://doi.org/10.18632/oncotarget.9239>
  - 20 Song K, Su W, Liu Y, Zhang J, Liang Q, Li N, et al. Identification of genes with universally upregulated or downregulated expressions in colorectal cancer. *J Gastroenterol Hepatol.* 2019;34:880–9. <https://doi.org/10.1111/jgh.14529>
  - 21 Bi L, Ma F, Tian R, Zhou Y, Lan W, Song Q, et al. AJUBA increases the cisplatin resistance through hippo pathway in cervical cancer. *Gene.* 2018;644:148–54. <https://doi.org/10.1016/j.gene.2017.11.017>
  - 22 Liang XH, Zhang GX, Zeng YB, Yang HF, Li WH, Liu QL, et al. LIM protein JUB promotes epithelial-mesenchymal transition in colorectal cancer. *Cancer Sci.* 2014;105:660–6. <https://doi.org/10.1111/cas.12404>
  - 23 Jia H, Song L, Cong Q, Wang J, Xu H, Chu Y, et al. The LIM protein AJUBA promotes colorectal cancer cell survival through suppression of JAK1/STAT1/IFIT2 network. *Oncogene.* 2017;36:2655–66. <https://doi.org/10.1038/onc.2016.418>
  - 24 Yang D, Hou T, Li L, Chu Y, Zhou F, Xu Y, et al. Smad1 promotes colorectal cancer cell migration through Ajuba transactivation. *Oncotarget.* 2017;8:110415–25. <https://doi.org/10.18632/oncotarget.22780>
  - 25 Zhang M, Singh R, Peng S, Mazumdar T, Sambandam V, Shen L, et al. Mutations of the LIM protein AJUBA mediate sensitivity of head and neck squamous cell carcinoma to treatment with cell-cycle inhibitors. *Cancer Lett.* 2017;392:71–82. <https://doi.org/10.1016/j.canlet.2017.01.024>
  - 26 Zhang B, Song L, Cai J, Li L, Xu H, Li M, et al. The LIM protein Ajuba/SP1 complex forms a feed forward loop to induce SP1 target genes and promote pancreatic cancer cell proliferation. *J Exp Clin Cancer Res.* 2019;38:205. <https://doi.org/10.1186/s13046-019-1203-2>
  - 27 Tanaka I, Osada H, Fujii M, Fukatsu A, Hida T, Horio Y, et al. LIM-domain protein AJUBA suppresses malignant mesothelioma cell proliferation via Hippo signaling cascade. *Oncogene.* 2015;34:73–83. <https://doi.org/10.1038/onc.2013.528>
  - 28 Liu M, Jiang K, Lin G, Liu P, Yan Y, Ye T, et al. Ajuba inhibits hepatocellular carcinoma cell growth via targeting of  $\beta$ -catenin and YAP signaling and is regulated by E3 ligase Hakai through neddylation. *J Exp Clin Cancer Res.* 2018;37:165. <https://doi.org/10.1186/s13046-018-0806-3>
  - 29 Jia L, Gui B, Zheng D, Decker KF, Tinay I, Tan M, et al. Androgen receptor-regulated miRNA-193a-3p

- targets AJUBA to promote prostate cancer cell migration. *Prostate*. 2017;**77**:1000–11. <https://doi.org/10.1002/pros.23356>
- 30 Du P, Huang P, Huang X, Li X, Feng Z, Li F, et al. Comprehensive genomic analysis of oesophageal squamous cell carcinoma reveals clinical relevance. *Sci Rep*. 2017;**7**:15324. <https://doi.org/10.1038/s41598-017-14909-5>
  - 31 Le Y, He Y, Bai M, Wang Y, Wu J, Yu L. Knockout of Ajuba attenuates the growth and migration of hepatocellular carcinoma cells. *Cytogenet Genome Res*. 2020;**160**:650–8. <https://doi.org/10.1159/000512264>
  - 32 Loforese G, Malinka T, Keogh A, Baier F, Simillion C, Montani M, et al. Impaired liver regeneration in aged mice can be rescued by silencing Hippo core kinases MST1 and MST2. *EMBO Mol Med*. 2017;**9**:46–60. <https://doi.org/10.15252/emmm.201506089>
  - 33 Tolba R, Kraus T, Liedtke C, Schwarz M, Weiskirchen R. Diethylnitrosamine (DEN)-induced carcinogenic liver injury in mice. *Lab Anim*. 2015;**49**:59–69. <https://doi.org/10.1177/0023677215570086>
  - 34 Scholten D, Trebicka J, Liedtke C, Weiskirchen R. The carbon tetrachloride model in mice. *Lab Anim*. 2015;**49**:4–11. <https://doi.org/10.1177/0023677215571192>
  - 35 Wu J, Wang ML, Xu Z, Qiu SL, Zhu JQ, Zhu DX. The role of TNF- $\alpha$  in the growth and differentiation of U937 cells induced by PMA and IFN- $\gamma$ . *Shi Yan Sheng Wu Xue Bao*. 1994;**27**:307–13.
  - 36 Song M-G, Ryoo I-G, Choi H-Y, Choi B-H, Kim S-T, Heo T-H, et al. NRF2 signaling negatively regulates phorbol-12-myristate-13-acetate (PMA)-induced differentiation of human monocytic U937 cells into pro-inflammatory macrophages. *PLoS One*. 2015;**10**:e0134235. <https://doi.org/10.1371/journal.pone.0134235>
  - 37 Kallas A, Pook M, Maimets M, Zimmermann K, Maimets T. Nocodazole treatment decreases expression of pluripotency markers Nanog and Oct4 in human embryonic stem cells. *PLoS One*. 2011;**6**:e19114. <https://doi.org/10.1371/journal.pone.0019114>
  - 38 Flomerfelt FA, Gress RE. Analysis of cell proliferation and homeostasis using EdU labeling. *Methods Mol Biol*. 2016;**1323**:211–20. [https://doi.org/10.1007/978-1-4939-2809-5\\_18](https://doi.org/10.1007/978-1-4939-2809-5_18)
  - 39 Weinstein JN, Collisson EA, Mills GB, Shaw KRM, Ozenberger BA, Ellrott K, et al. The cancer genome atlas pan-cancer analysis project. *Nat Genet*. 2013;**45**:1113–20. <https://doi.org/10.1038/ng.2764>
  - 40 Dommann N, Sánchez-Taltavull D, Eggs L, Birrer F, Brodie T, Salm L, et al. The LIM protein Ajuba augments tumor metastasis in colon cancer. *Cancers (Basel)*. 2020;**12**:1913. <https://doi.org/10.3390/cancers12071913>
  - 41 Szklarczyk D, Gable AL, Nastou KC, Lyon D, Kirsch R, Pyysalo S, et al. The STRING database in 2021: customizable protein–protein networks, and functional characterization of user-uploaded gene/measurement sets. *Nucleic Acids Res*. 2021;**49**:D605–12.
  - 42 Chen G, Deng X. Cell synchronization by double thymidine block. *Bio Protoc*. 2018;**8**:e2994. <https://doi.org/10.21769/BioProtoc.2994>
  - 43 Macheret M, Bhowmick R, Sobkowiak K, Padayachy L, Mailler J, Hickson ID, et al. High-resolution mapping of mitotic DNA synthesis regions and common fragile sites in the human genome through direct sequencing. *Cell Res*. 2020;**30**:997–1008. <https://doi.org/10.1038/s41422-020-0358-x>
  - 44 Macheret M, Halazonetis TD. Intragenic origins due to short G1 phases underlie oncogene-induced DNA replication stress. *Nature*. 2018;**555**:112–6. <https://doi.org/10.1038/nature25507>
  - 45 Stark C, Breitkreutz BJ, Reguly T, Boucher L, Breitkreutz A, Tyers M. BioGRID: a general repository for interaction datasets. *Nucleic Acids Res*. 2006;**34**:D535–9. <https://doi.org/10.1093/nar/gkj109>
  - 46 Das Thakur M, Feng Y, Jagannathan R, Seppa MJ, Skeath JB, Longmore GD. Ajuba LIM proteins are negative regulators of the Hippo signaling pathway. *Curr Biol*. 2010;**20**:657–62. <https://doi.org/10.1016/j.cub.2010.02.035>
  - 47 Liu VF, Weaver DT. The ionizing radiation-induced replication protein A phosphorylation response differs between ataxia telangiectasia and normal human cells. *Mol Cell Biol*. 1993;**13**:7222–31. <https://doi.org/10.1128/mcb.13.12.7222>
  - 48 Zou Y, Liu Y, Wu X, Shell SM. Functions of human replication protein A (RPA): from DNA replication to DNA damage and stress responses. *J Cell Physiol*. 2006;**208**:267–73. <https://doi.org/10.1002/jcp.20622>
  - 49 Loganathan SK, Schleicher K, Malik A, Quevedo R, Langille E, Teng K, et al. Rare driver mutations in head and neck squamous cell carcinomas converge on NOTCH signaling. *Science*. 2020;**367**:1264–9. <https://doi.org/10.1126/science.aax0902>
  - 50 Fagerberg L, Hallström BM, Oksvold P, Kampf C, Djureinovic D, Odeberg J, et al. Analysis of the human tissue-specific expression by genome-wide integration of transcriptomics and antibody-based proteomics. *Mol Cell Proteomics*. 2014;**13**:397–406. <https://doi.org/10.1074/mcp.M113.035600>
  - 51 Schleicher K, Schramek D. AJUBA: a regulator of epidermal homeostasis and cancer. *Exp Dermatol*. 2020;**30**:546–59. <https://doi.org/10.1111/exd.14272>
  - 52 Pratt SJ, Eppler H, Ward M, Feng Y, Braga VM, Longmore GD. The LIM protein Ajuba influences p130Cas localization and Rac1 activity during cell migration. *J Cell Biol*. 2005;**168**:813–24. <https://doi.org/10.1083/jcb.200406083>
  - 53 Kanungo J, Pratt SJ, Marie H, Longmore GD. Ajuba, a cytosolic LIM protein, shuttles into the nucleus and



- affects embryonal cell proliferation and fate decisions. *Mol Biol Cell*. 2000;**11**:3299–313.
- 54 Crevel I, Crevel G, Gostan T, de Renty C, Coulon V, Cotterill S. Decreased MCM2-6 in *Drosophila* S2 cells does not generate significant DNA damage or cause a marked increase in sensitivity to replication interference. *PLoS One*. 2011;**6**:e27101. <https://doi.org/10.1371/journal.pone.0027101>
  - 55 Zhou BB, Elledge SJ. The DNA damage response: putting checkpoints in perspective. *Nature*. 2000;**408**:433–9. <https://doi.org/10.1038/35044005>
  - 56 Kalan S, Matveyenko A, Loayza D. LIM protein Ajuba participates in the repression of the ATR-mediated DNA damage response. *Front Genet*. 2013;**4**:95. <https://doi.org/10.3389/fgene.2013.00095>
  - 57 Enders GH. Expanded roles for Chk1 in genome maintenance. *J Biol Chem*. 2008;**283**:17749–52. <https://doi.org/10.1074/jbc.R800021200>
  - 58 Dong S, Chen QL, Song YN, Sun Y, Wei B, Li XY, et al. Mechanisms of CCl<sub>4</sub>-induced liver fibrosis with combined transcriptomic and proteomic analysis. *J Toxicol Sci*. 2016;**41**:561–72. <https://doi.org/10.2131/jts.41.561>
  - 59 Heffelfinger SC, Hawkins HH, Barrish J, Taylor L, Darlington GJ. SK HEP-1: a human cell line of endothelial origin. *In Vitro Cell Dev Biol*. 1992;**28A**:136–42. <https://doi.org/10.1007/BF02631017>
  - 60 Boyault S, Rickman DS, de Reyniès A, Balabaud C, Rebouissou S, Jeannot E, et al. Transcriptome classification of HCC is related to gene alterations and to new therapeutic targets. *Hepatology*. 2007;**45**:42–52. <https://doi.org/10.1002/hep.21467>
  - 61 Rebouissou S, Zucman-Rossi J, Moreau R, Qiu Z, Hui L. Note of caution: contaminations of hepatocellular cell lines. *J Hepatol*. 2017;**67**:896–7. <https://doi.org/10.1016/j.jhep.2017.08.002>
  - 62 Portmann S, Fahrner R, Lechleiter A, Keogh A, Overney S, Laemmle A, et al. Antitumor effect of SIRT1 inhibition in human HCC tumor models in vitro and in vivo. *Mol Cancer Ther*. 2013;**12**:499–508. <https://doi.org/10.1158/1535-7163.MCT-12-0700>
  - 63 Karkampouna S, van der Helm D, Gray PC, Chen L, Klima I, Grosjean J, et al. CRIPTO promotes an aggressive tumour phenotype and resistance to treatment in hepatocellular carcinoma. *J Pathol*. 2018;**245**:297–310. <https://doi.org/10.1002/path.5083>
  - 64 Therneau TM, Grambsch PM. Modeling survival data: extending the cox model. New York, NY: Springer; 2000.
  - 65 Way M. R package version 1.0; 2016. Available from: <https://rdrr.io/github/michaelway/ggkm/>
  - 66 Aida T, Chiyo K, Usami T, Ishikubo H, Imahashi R, Wada Y, et al. Cloning-free CRISPR/Cas system facilitates functional cassette knock-in in mice. *Genome Biol*. 2015;**16**:87. <https://doi.org/10.1186/s13059-015-0653-x>
  - 67 National Library of Medicine. Tool for finding specific primers National Center for Biotechnology Information.
  - 68 Franken NA, Rodermond HM, Stap J, Haveman J, van Bree C. Clonogenic assay of cells in vitro. *Nat Protoc*. 2006;**1**:2315–9. <https://doi.org/10.1038/nprot.2006.339>
  - 69 Brown ZJ, Yu SJ, Heinrich B, Ma C, Fu Q, Sandhu M, et al. Indoleamine 2,3-dioxygenase provides adaptive resistance to immune checkpoint inhibitors in hepatocellular carcinoma. *Cancer Immunol Immunother*. 2018;**67**:1305–15. <https://doi.org/10.1007/s00262-018-2190-4>
  - 70 Gavini J, Dommann N, Jakob MO, Keogh A, Bouchez LC, Karkampouna S, et al. Verteporfin-induced lysosomal compartment dysregulation potentiates the effect of sorafenib in hepatocellular carcinoma. *Cell Death Dis*. 2019;**10**:749. <https://doi.org/10.1038/s41419-019-1989-z>
  - 71 Peer VD. Venn diagrams for Bioinformatics & Evolutionary Genomics Web tool Diagrams CadeV. Available from: <http://bioinformatics.psb.ugent.be/webtools/Venn/>
  - 72 Zhou Y, Zhou B, Pache L, Chang M, Khodabakhshi AH, Tanaseichuk O, et al. Metascape provides a biologist-oriented resource for the analysis of systems-level datasets. *Nat Commun*. 2019;**10**:1523. <https://doi.org/10.1038/s41467-019-09234-6>
  - 73 Mariotti LG, Pirovano G, Savage KI, Ghita M, Ottolenghi A, Prise KM, et al. Use of the  $\gamma$ -H2AX assay to investigate DNA repair dynamics following multiple radiation exposures. *PLoS One*. 2013;**8**:e79541. <https://doi.org/10.1371/journal.pone.0079541>
  - 74 Wickham H. ggplot2: elegant graphics for data analysis. New York, NY: Springer Verlag; 2016.

## Supporting information

Additional supporting information may be found online in the Supporting Information section at the end of the article.

**Fig. S1.** Western blot analysis of Ajuba expression in mouse liver tissue before and after different time points post partial hepatectomy.

**Fig. S2.** Western blot analysis of Ajuba protein in human primary hepatocytes and liver cancer cell lines.

**Fig. S3.** Ajuba mRNA expression level measured by RT-qPCR in U-937 monocyte cell line treated for 3 days with DMSO (50ng/ml,) PMA (160nM) or Nocodazole (100ng/ml).

**Fig. S4.** Confocal immunofluorescent image of an actively proliferating human HCC derived organoids with 2h EdU incorporation and Dapi staining.

**Fig. S5.** (A) Ajuba sequence with Exon 1-8 highlighted. (B) CRISPR/Cas9 Ajuba KO strategy using 2



guide RNA targeting exon 1 and creating a 647bp deletion. (C) Genotyping of the founder lines FL1 and FL2. (D) Number of exact base pair deletion in the different founder lines was assessed using codon code aligner and sanger sequencing. (E) Family tree of F1 generation Founder line 1. Graph displaying the percentages of KO mice generated in generation F2 (N = 258), Chi-squared goodness of fit test was performed comparing found genotypes with expected mendelian ratios, \*\*\*\* denotes p-value < 2.2e-16. (F) Family tree of F1 generation Founder line 2. Graph displaying the percentages of KO mice generated in generation F2 (N = 142) Chi-squared goodness of fit test was performed comparing found genotypes with expected mendelian ratios, \*\*\*\* denotes p-value = 5.256e-11. (G) Summary table of the genotyped mice as well as the expected mendelian ratios.

**Fig. S6.** Ajuba mRNA expression in Huh7 cell lines after lentiviral transduction with shScrambled, shAjuba1 and shAjuba2.

**Fig. S7.** Tumor growth of subcutaneous syngenic tumor was measured over a time span of 11 days in

C57BL/6 mice, injected with HCC cell line (RIL-175), where Ajuba was previously depleted.

**Fig. S8.** (A) String analysis of Ajuba and its potential binding partners identified by Mass spectrometry. (B) Pathway enrichment analysis of all Class I and Class II proteins, using Metascape and displaying the 20 most significant pathways.

**Fig. S9.** Pie chart displaying the subcellular locations associated with the potential Ajuba binding partners found with Mass spectrometry.

**Fig. S10.** (A) Pathway enrichment analysis using metascape of Class I (A) and Class II (B) proteins identified by MS. 20 most significant pathways are displayed.

**Fig. S11.** Survival curves of the percentage of colonies of Huh7 cell lines irradiated with 0-6 Gray (Gamma-cell40).

**Fig. S12.** Percentage of γH2Ax positive cells detected after 2 Gray irradiation at two different time points (2h and 4h).

**Table S1.** Mass spectrometry output.

**Table S2.** Mass spectrometry Class I and Class II.